Journal of Asian Earth Sciences 146 (2017) 304–316

Contents lists available at ScienceDirect

Journal of Asian Earth Sciences

journal homepage: www.elsevier.com/locate/jseaes

Full length article

Paleoseismology and slip rate of the western Tianjingshan fault of NE Tibet, China

Xinnan Li[a,b,c], Chuanyou Li[b,*], Steven G. Wesnousky[c], Peizhen Zhang[a,d], Wenjun Zheng[a,d], Ian K.D. Pierce[c], Xuguang Wang[b]

[a] State Key Laboratory of Earthquake Dynamics, Institute of Geology, China Earthquake Administration, Beijing 100029, China
[b] Key Laboratory of Active Tectonics and Volcano, Institute of Geology, China Earthquake Administration, Beijing 100029, China
[c] Center for Neotectonic Studies, Mail Stop 169, University of Nevada, Reno, Nevada 89557, USA
[d] School of Earth Science and Geological Engineering, Sun Yat-Sen University, Guangzhou 510275, China

ARTICLE INFO

Keywords:
Tianjingshan fault
Paleoseismology
Slip rate
NE Tibet
Tectonic deformation

ABSTRACT

We present results from a detailed investigation of the horizontal displacement distribution, timing of paleoearthquakes and left-lateral slip rate on the western Tianjingshan fault. Measurements of 240 offset streams and ridges confirm that the fault is left-lateral and record evidence of repeated ~3–4 m coseismic offsets along the 60–km–long fault. This suggests that ~6 earthquakes may have occurred along the entire western Tianjingshan fault with repeated occurrence of earthquakes of Mw 7.2–7.5. Structural and stratigraphic relationships exposed in our five trenches in combination with previously reported studies further indicate that the fault has ruptured in as many as six paleoearthquakes since the late Quaternary. Paleoseismic data show that the average recurrence interval for Holocene earthquakes is approximately 5,000 yr. The most recent earthquake along the western Tianjingshan fault occurred ~1.2 ± 0.1 kyr BP, indicating that this fault segment did not rupture in the M 7.5 historical earthquake of 1709 that ruptured the central Tianjingshan fault. We estimate that the Holocene slip rate of the western Tianjingshan fault is ~1.1–1.2 mm/yr based on measurements of the age and offset of stream channels. Compared with the relatively fast slip rate of the Haiyuan fault (~4–6 mm/yr), we suggest that the Tianjingshan fault acts as an essential active fault accommodating the sinistral displacement and crustal shortening deformation in NE Tibet.

1. Introduction

The major left-lateral Altyn-Tagh and Haiyuan faults strike along the northern and northeastern margins of the Tibetan Plateau, respectively (Fig. 1A). The Tianjingshan fault splays eastward off the north side of the Haiyuan fault (Fig. 1B) and marks the northernmost strike-slip fault boundary associated with the northeast margin of the Tibetan Plateau. The Tianjingshan fault is defined by a series of discontinuous Holocene active fault traces, which extends for a distance of 240 km, approximately from Gulang in the west to Tongxin city in the east. The fault is divided into four sections based on fault geometry and geomorphology (Li and Li, 2015); from west to east, these are the northern Changlingshan fault (N-CLF), and the western (W-TJSF), central (C-TJSF), and eastern (E-TJSF) Tianjingshan faults (Fig. 1B). On October 14, 1709, the M 7.5 Zhongwei (Ningxia) earthquake killed > 2000 people and produced a left-lateral surface rupture ~30–60 km long along a portion of the central Tianjingshan fault (C-TJSF) (W.Q. Zhang et al., 1988; Zhang et al., 2015; Fig. 1B). Numerous studies have described the well-preserved surface ruptures (Nie and Lin, 1993; W.Q. Zhang et al., 1988), established the average recurrence intervals (2000–4000 yr, Min et al., 2001; Zhou and Liu, 1987; Wang et al., 1990), and defined the slip rates (~2 ± 0.5 mm/yr; Chai et al., 1997; Li, 2005) of the C-TJSF.

The 60-km-long western Tianjingshan fault (W-TJSF) has received less attention than the C-TJSF. Chai et al. (2003) observed that the W-TJSF traverses, but does not cut, the Great Wall of China (built in 1598 CE during the Ming Dynasty) and with geomorphic observations concluded that the most recent rupture along the W-TJSF occurred more than 400 yr ago and did not rupture in the 1709 earthquake. The W-TJSF has an average strike of ~N90°E and is composed of five subparallel fault strands separated by pull-apart basins of different sizes (Du et al., 2007). The individual fault strands are designated from west to east as F1 to F5 (Fig. 1C). The average strike of the western Tianjingshan fault is about N90°E. It remains unknown whether the relative

* Corresponding author at: Key Laboratory of Active Tectonics and Volcano, Institute of Geology, China Earthquake Administration, No.1 Huayanli, Chaoyang District, Beijing 100029, China.
E-mail address: chuanyou@ies.ac.cn (C. Li).

http://dx.doi.org/10.1016/j.jseaes.2017.04.031
Received 10 November 2016; Received in revised form 17 April 2017; Accepted 18 April 2017
Available online 31 May 2017
1367-9120/

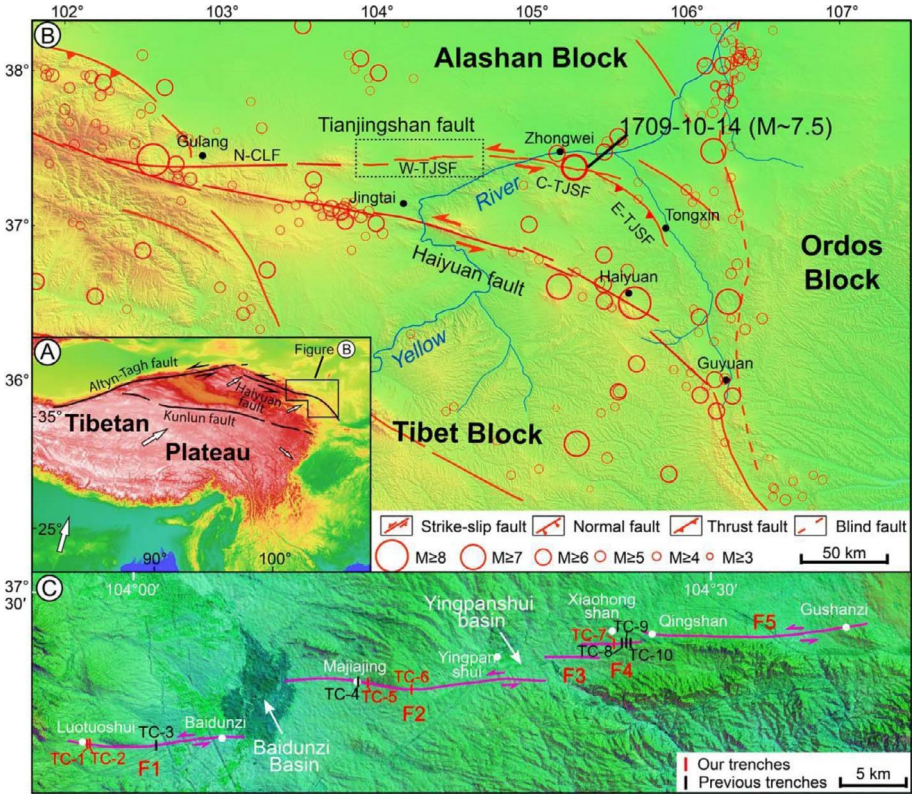

Fig. 1. Tectonic setting of the study area. (A) Regional tectonic map of the study area on the Tibetan Plateau. The black box shows the location of (B). (B) Topographic and tectonic map of northeastern Tibet showing the major active faults. Sections of the fault discussed in the text are labeled: W-TJSF, western Tianjingshan fault; C-TJSF, central Tianjingshan fault; E-TJSF, eastern Tianjingshan fault; NCLF, northern Changlingshan fault; Red circles are epicenters of earthquakes (M ≥ 3) from the China Earthquake Networks Center catalog (and from Gu et al. (1983). The epicenter of the 1709 M 7.5 earthquake on the C-TJSF is highlighted. Dashed black box shows the location of (C). (C) Active fault traces of the W-TJSF: F1, Jingtai subsegment; F2, Guanguanling subsegment; F3, Shajing subsegment; F4, Zhongwei subsegment; F5, Qinshan–Gushanzi subsegment. Red bars are trenches excavated in this study. Black bars are trenches excavated in previous studies. Numbers correspond to trenches TC-1 through TC-10. (For interpretation of the references to colour in this figure legend, the reader is referred to the web version of this article.)

scarcity of instrumentally recorded earthquakes along the W-TJSF, between Luotuoshui and Gushanzi (Fig. 1B and C), implies that the fault is locked, and therefore might pose a significant potential seismic hazard to the heavily populated Jingtai and Zhongwei regions, or reflects that the fault is experiencing a seismically calm period, and would not produce a large earthquake in the near future.

In this paper, we present geomorphic evidence of repeated slip at more than 16 sites along the traces of the western Tianjingshan fault (W-TJSF). We then combine new paleoseismic observations, obtained by trenching, with previously reported observations (Chen et al., 2006; Du et al., 2007; Unpublished results, IGCEA et al., 2003; Min et al., 2001) to interpret the past rupture history and the recurrence intervals of large surface-rupturing earthquakes on the W-TJSF. Additionally, we measure the age and offset of an older stream channel to estimate the W-TJSF slip rate. The results provide a basis to discuss the behavior of the fault within the context of existing earthquake recurrence models and the tectonic role of the fault along the northeast margin of the Tibetan Plateau.

2. Methods

We measured offset geomorphic features along the W-TJSF using tape measures and laser rangefinders in the field, as well as Google Earth imagery, and structure-from-motion (SfM) models (Supplementary Material S1 and Figs. S1–S3). Fault traces F3 and F5 are typically modified by surface mining, so our measurements are limited to those made along segments F1, F2, and F4. The offset measurement results are presented in Section 3.1. Five trenches (TC-1, TC-2, TC-5, TC-6, and TC-7) were excavated, using both hand tools and machine excavators, across the active fault scarps, mainly along the F1, F2, and F4 segments. The location of each trench is shown in Fig. 1C. Before trenching, the fault-trace geometry and surface geomorphic units were mapped and topographic profiles were measured across the fault scarps at each site. The walls of each trench were scraped and cleaned and the exposures were marked with a 1-m string grid prior to logging. The sedimentary layers in each trench were differentiated as individual units based on color, grain size, sorting, texture, bedding thickness, and other features such as liquefaction (Table S1). The sequence of ground-rupturing events was then defined on the basis of stratal cross-cutting relationships, sediment thickness changes, soft-sediment deformation, fissures, and sand liquefaction. In each trench, the interpreted paleoearthquakes are designated as E1, E2, etc., with E1 being the youngest. Optically stimulated luminescence (OSL) ages of sediment samples collected from the trenches are used to constrain the ages of the stratigraphic units, and hence the interpreted events. All samples were processed and analyzed in the Luminescence Dating Laboratory at the State Key Laboratory of Earthquake Dynamics, Institute of Geology, China Earthquake Administration (CEA), Beijing, using conventional pretreatment techniques (see Lu et al. (2007) and Yang et al. (2012) for the detailed experimental procedures). The OSL results and details of methodology are summarized in Supplementary Material S1 and Table S2.

3. Results

3.1. Geomorphic evidence for paleoearthquakes from offset measurements

Numerous offset geomorphic features can be observed, both in the field and from Google Earth imagery, along the W-TJSF. For example, Fig. 2 shows that a series of stream channels emerging from small hills composed of late Neogene and early Pleistocene sediments are displaced by the fault. The enlarged circles in Fig. 2 indicate recent left-lateral stream offsets. As a result, these offset features of different sizes offer us a good opportunity to better document the seismic behavior and the occurrence of past large earthquakes on the W-TJSF.

The 240 offset measurements are summarized in Supplementary Table 3. To quantitatively determine the relationship between along-strike offset distribution and individual paleoearthquakes, we plot our offset measurements as a function of distance along each fault segment (Fig. 3A). In Fig. 3A, symbols with shaded background connected by vertical dashed lines are measurements of multiple offsets made at the same site; whereas, sites exhibiting only one single offset are marked by

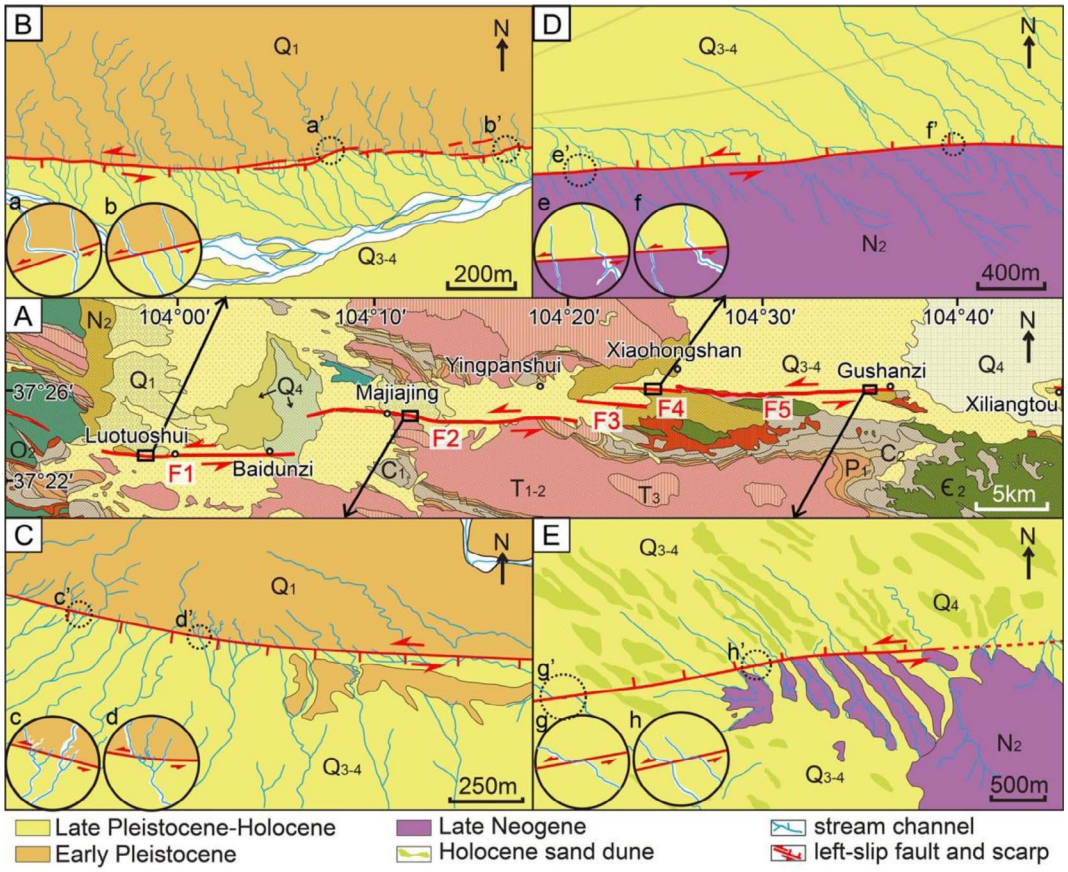

Fig. 2. Geological and geomorphological features of the W-TJSF. (A) Geological map and fault traces of the W-TJSF. Modified from Unpublished results, IGCEA et al. (2003). Small black boxes show the geomorphological mapping areas in B–E. (B–E) Surficial geologic maps produced using Google Earth imagery and field observations. Circles a–h, located in the lower-left corners of (B)–(E) show enlarged maps of left-laterally displaced stream channels at sites marked by dashed black circles a′–h′ in respective subfigures.

unconnected symbols without a shaded background. The sum of the observations in Fig. 3A is plotted as a histogram in Fig. 3B. We observe peaks in the histogram, separated on average by 3–4 m, and interpret that each peak may represent the occurrence of a large earthquake rupturing the entire 60–km length of the W-TJSF. This interpretation is based on the observation that earthquake ruptures appear to propagate easily across 3–4 km releasing steps (Wesnousky, 2006) and is supported by our trenching results, which show that at least the most

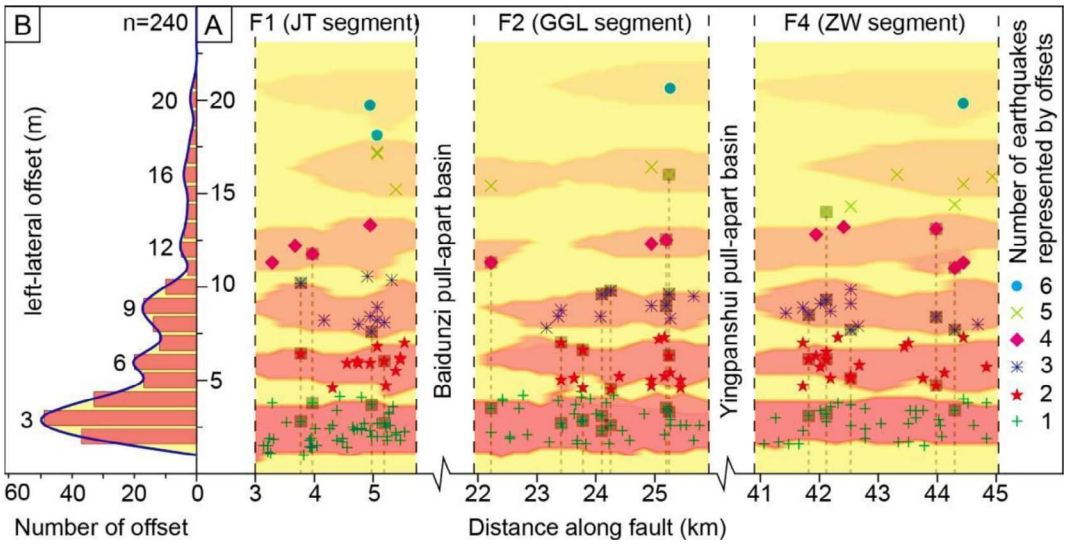

Fig. 3. Relationship between stream offset distribution and individual paleoearthquakes along the strike of the W-TJSF. (A) Plot of 240 horizontal offset measurements distributed as a function of distance along strike for the three major subsegments of the W-TJSF. Offset values are color coded to highlight displacements interpreted as resulting from the same number of paleoearthquakes. Vertical dashed lines and symbols with shaded background indicate sites with repeated offset at the individual site. (B) Frequency counts for the 240 offset measurements (see Supplementary Table 2), calculated using a non-overlapping sliding window in steps of 1 m, and histogram showing the number of offsets per m displacement. Each peak (~3, 6, 9, 12, 16, and 20 m) on the fitting curve is interpreted to represent the average offset of multiple earthquakes. The difference between average peak values is approximately 3 m. (For interpretation of the references to colour in this figure legend, the reader is referred to the web version of this article.)

recent earthquake ruptured the entire W-TJSF (see Section 4). In addition, a similar peak spacing was observed for other faults and was interpreted as the average slip during each earthquake (e.g. Klinger et al., 2011; Zielke et al., 2010), so we infer that similar fault behavior may occur on the W-TJSF. The smallest observable offsets are interpreted to correspond to the most recent earthquake, as evidenced by a stream channel that was left-laterally displaced by 2.7 m across the newly-ruptured fault strand f3 exposed in TC-5 trench (see Section 3.2.2), and successively larger offset groups are interpreted to record the cumulative slip of prior events. These interpretations assume that the production rate of geomorphic features capable of recording fault offset is much higher than the frequency of surface-rupturing earthquakes (Zielke et al., 2015). The 129 single-event offsets, attributed to the most recent earthquake, record an average coseismic slip of 3 ± 1.5 m. Consequently, the distinct peaks at ~6 and ~9 m may represent the penultimate and antepenultimate earthquakes due to repetition of earthquakes producing ~3 m coseismic offsets. Peaks at ~12, ~16, and ~20 m are likely the result of the cumulative slip of four to six entire-W-TJSF-rupturing earthquakes. Despite the uncertainty arising from the decreasing number of larger offset measurements, our observations appear to support the idea that the slip distribution is similar for each repeated earthquake along the W-TJSF.

3.2. Paleoseismic evidence from trenching investigations

To assess the timing of earthquakes responsible for each peak in the histogram shown in Fig. 3B, we use the structural, stratigraphic, and OSL age relationships observed in the five trenches (TC-1, TC-2, TC-5, TC-6, and TC-7) excavated across the fault (Fig. 1C). Trench sites TC-2, TC-5, and TC-7 are described in the sections below (see Supplementary Material S2 and Figs. S4–S6 for detail of TC-1 and TC-6). Detailed descriptions of the sedimentary units in the trench exposures and the OSL ages of all samples collected from the trenches are summarized in Supplementary Tables 1 and 2, respectively.

3.2.1. TC-2

The location and geomorphic context of trench site TC-2 are shown in Figs. 1C and 4C. The trench log presented in Fig. 5 shows a sequence of alluvial layers overlain by finer–grained aeolian loess. The sedimentary sequence is cut by four fault strands: f1, f2, f3, and f4. The stratigraphic and tectonic relationships appear to show only a single earthquake displacement in the TC-2 trench. This event produced folding and thrust faulting of units U1-1/2, U1-2, and U1-3 along fault zone f3-4, which dies out upwards in unit U1-4; these units are overlain by undeformed unit U2 (Fig. 6A). The E1 event has also been identified as the termination of fault zone f1-2 in unit U1-4 toward the top of the exposed surface (Fig. 6B). Although we cannot completely rule out the possibility that f3-4 displacement may represent an event older than f1-2 displacement in the TC-2 trench, it is more likely that fault strands f1, f2, f3, and f4 ruptured simultaneously because in trench TC-1, approximately 200 m west of trench TC-2, only one earthquake displacement is similarly observed. Sample TJSH-50, taken from the base of unit U1-4, gave an 4.4 ± 0.3 kyr BP, which represents the upper limit of the event horizon; sample TJSH-51, taken from the top of unit U1-4, gave an age of 0.2 ± 0.1 kyr BP, which indicates the lower chronological limit for the most recent earthquake (E1). Therefore, E1 is likely to have occurred within 0.2–4.4 kyr BP.

3.2.2. TC-5

At this trench site (location shown in Figs. 1C and 7A and B), the fault trace strikes S105°E and can be recognized on satellite imagery as well as in the field as a clear, single, linear trace that offsets a large number of streams along the Guanguanling subsegment (F2). We excavated a 14-m-long trench across a south-facing scarp, located approximately 700 m east of Majiajing, on the F2 subsegment. At this site, the fault trace cuts across a late Pleistocene–Holocene alluvial fan, and left-laterally displaces a young stream by ~2.7 m and an older stream by ~11.7 m to the west of our trench (Fig. 7C). Here, the scarp height is up to ~0.80 m, varying along strike between approximately 0.3 and 2.8 m, and the trench exposes, from oldest to youngest, a sequence of late Pleistocene and Holocene sedimentary layers, designated as units U1 through U11 (Fig. 8). The sequence is cut entirely or in part by seven fault strands, designated as f1 to f7 (Fig. 8).

We identified at least four paleoseismic events, designated as E1, E2, E3, and E4 as a function of increasing age, and we discuss here the evidence for each event in chronological order. The main fault zone consists of fault strands f3 to f7, all showing generally down-to-the-south displacement. Strand f3 extends highest in the section to where it

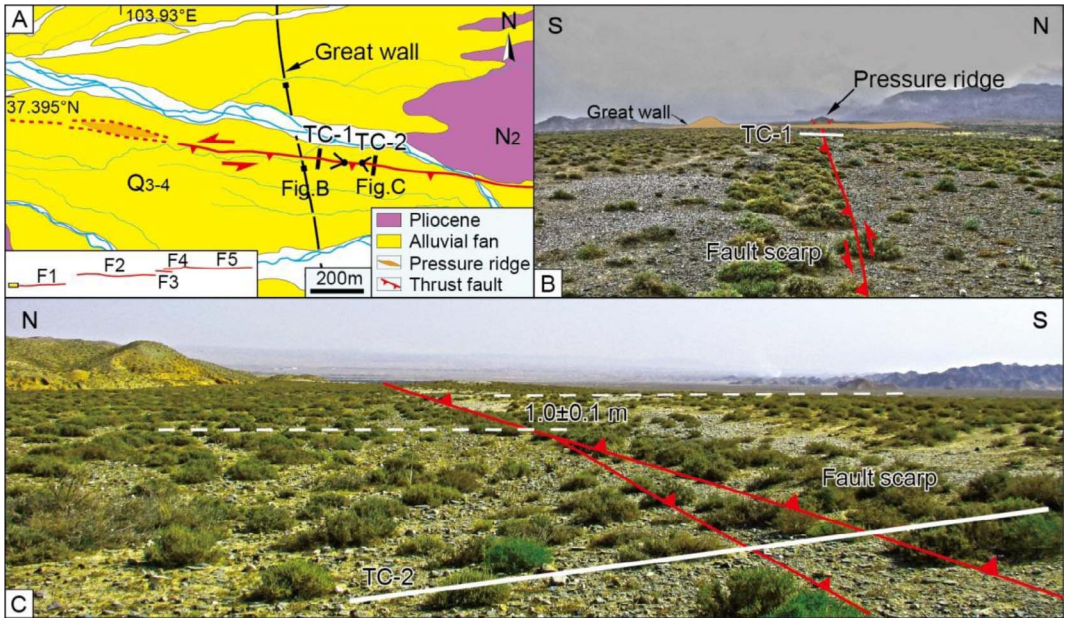

Fig. 4. Geomorphological mapping and features of the westernmost portion of F1 (Jingtai subsegment). (A) Morphotectonic map showing the fault trace, geomorphological units, and stream channels. Note that the fault trace terminates near the pressure ridge and the Great Wall (1598 CE) was not faulted by the surface trace. Location is shown in the lower-left corner sketch map. Black bars indicate the trench locations shown in (B) and (C). (B) Photograph showing the fault scarp truncating the youngest alluvial fan, trench site TC-1 (37.393046°N, 103.938413°E), and the relation between fault trace and the Great Wall. (C) View of north-facing scarp with a height of ~1 m and trench site TC-2 (37.392895°N, 103.940273°E).

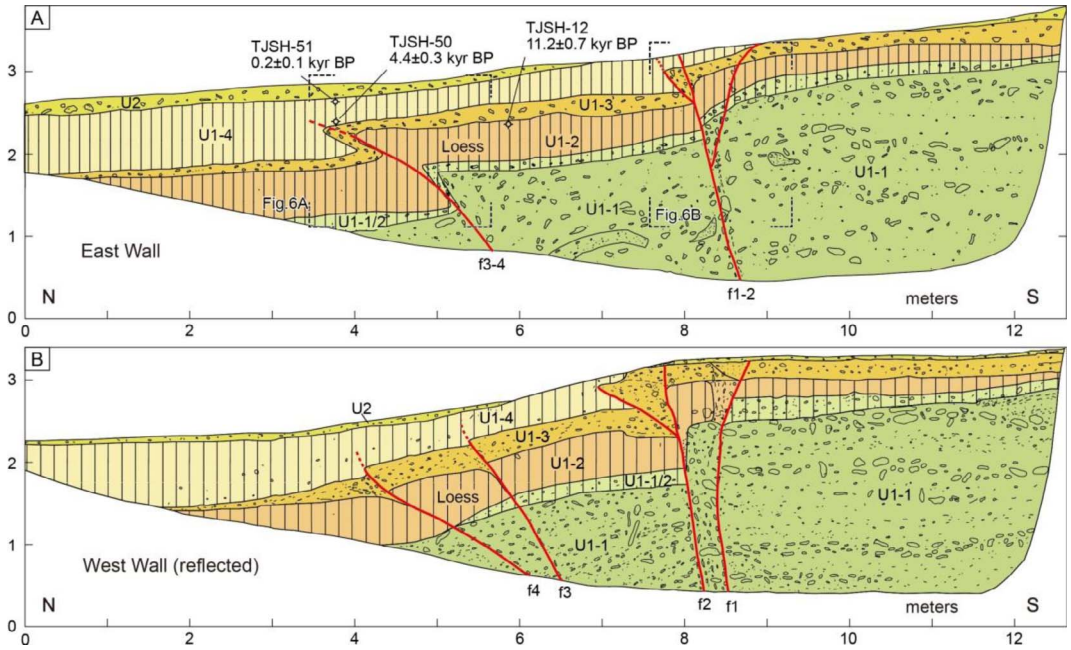

Fig. 5. Trench logs and dated stratigraphy of the east (A) and west (B, reflected) walls of TC-2. Red lines mark the faults, which form two major fault zones. The stratigraphy of TC-2 is similar to that observed in TC-1 (see detail in Table S1). Stratigraphic positions of OSL samples are shown by black circles. Dashed corners on the east wall of the trench (A) define areas that are further enlarged in Fig. 6 to show details of the stratigraphic units and cross-cutting relationships. See Section 3.2.1 for descriptions of evidence for the interpreted earthquake event E1. (For interpretation of the references to colour in this figure legend, the reader is referred to the web version of this article.)

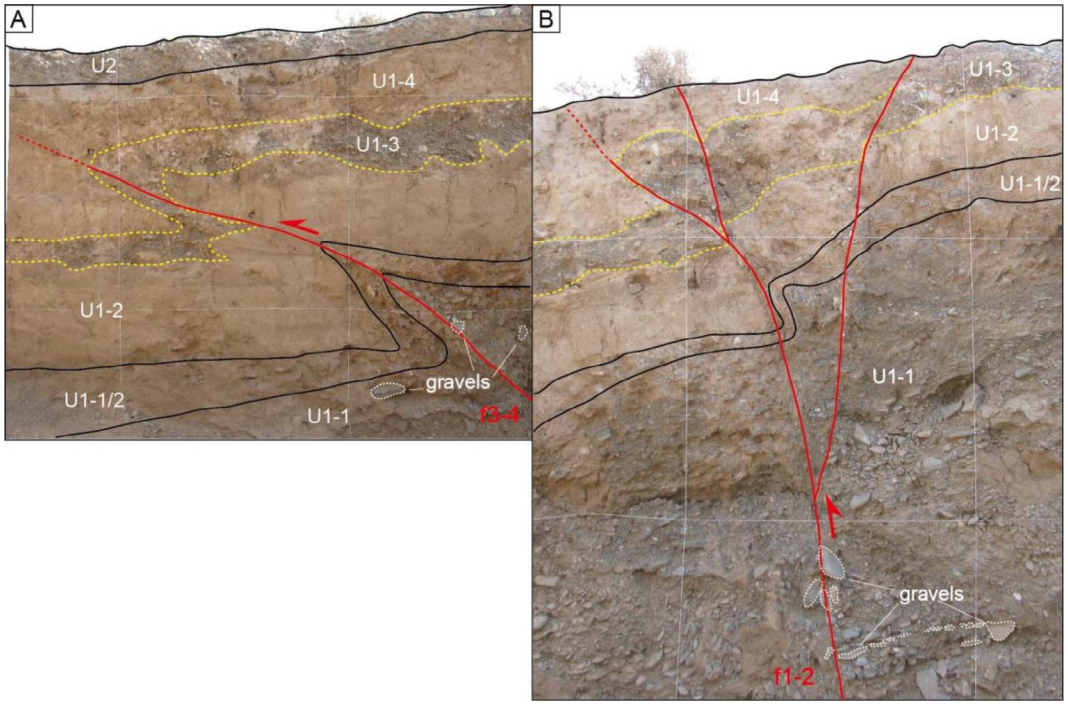

Fig. 6. Photomosaic of part of the west wall of TC-2 showing evidence for the interpreted earthquake event E1. (A) Fault strand f3-4, which folded units U1-1/2 to U1-3 and terminated within U1-4, provides evidence for E1. (B) Further evidence for E1 is provided by fault strand f1-2, which ruptured the ground surface. Note that the total vertical displacement of E1 is approximately 1 m, consistent with that measured across the fault scarp, suggesting that the youngest alluvial fan may only record the most recent earthquake event.

is capped by a thin unbroken layer, unit U11, and thus records the most recent displacement, paleoearthquake E1 in the exposure. OSL ages for samples taken from the unbroken unit U11 and the broken layer U10 place the time of last displacement on f3 at between 1.7 ± 0.2 kyr BP (TJSH-66) and 3.5 ± 0.4 kyr BP (TJSH-29). The apparent vertical offset on f3 is approximately 0.1–0.15 m across units U4 to U10, but the sense of displacement reverses and unit thicknesses vary across f3 in the lower units U1 and U3, suggesting that a component of the offset is strike-slip.

The penultimate earthquake (E2) is recorded by fault strands f4 and f6, which project upward and offset the base of unit U9, but do not offset the upper contact of unit U9. The lower contact of U10 is flat, suggesting that some amount of erosion of U9 occurred before U10 was deposited. Assuming that OSL sample TJSH-28, taken from the base of U9, was deposited prior to the last displacement on f4 and f6, it is interpreted that displacement on f4 and f6 occurred simultaneously after

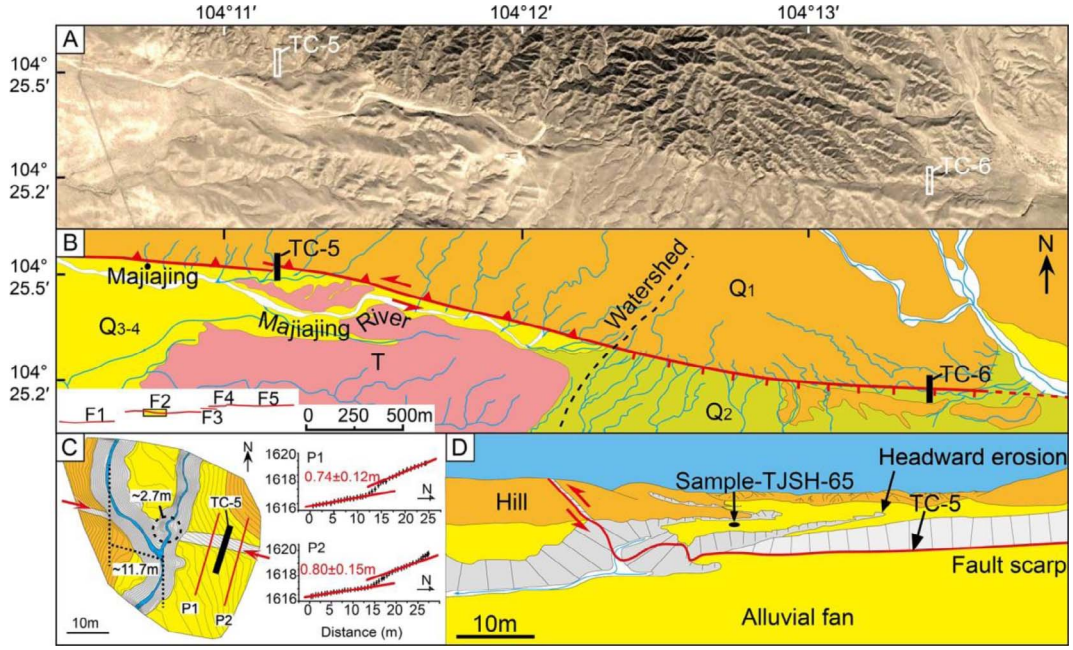

Fig. 7. Geomorphological mapping and features of the central portion of F2 (Guanguanling subsegment). (A) Google Earth imagery showing the central portion of F2, with precision of 10 m. (B) Corresponding morphotectonic map showing the fault trace, geomorphological units, and stream channels. Location is shown in the lower-left corner sketch map. Black box in the lower-left corner map indicates the trench location shown in (C). (C) Topographic map showing the fault scarp, offset channels, and TC-5 trench site. Contour interval is 0.2 m. Profiles (P1 and P2) across the fault zone show that the height of the scarp is ~0.8 m. (D) North-looking view of the interpreted faulted landscape at the trench site (37.425573°N, 104.186135°E). The alluvial fan is incised by the older (left) and younger (right) stream channels. Location of pit OSL sample TJSH-65 is shown by the black circle and arrow.

8.9 ± 0.8 kyr BP (TJSF-28) and before 3.5 ± 0.4 kyr BP, which is the age of sample TJSH-29 taken from the base of overlying unit U10 (Figs. 8 and 9A).

Displacements on fault strands f1 and f2 are interpreted to record an antepenultimate event (E3). Each strand projects upward from the base of the trench into the footwall and displaces the base of unit U7 where, together, they form a buried graben (Figs. 8 and 9B and C). However, neither strand f1 or f2 projects through to the upper contact of unit U7. The age of displacement on strands f1 and f2 clearly postdates deposition of unit U6, dated at 25.6 ± 1.4 kyr BP from OSL sample TJSH-31. Placing an upper bound on the timing of the antepenultimate event is problematic. The deposition of OSL sample TJSH-59, near the base of unit U7, may have occurred either before or after the displacement on underlying faults f1 and f2, and its position with respect to the fault

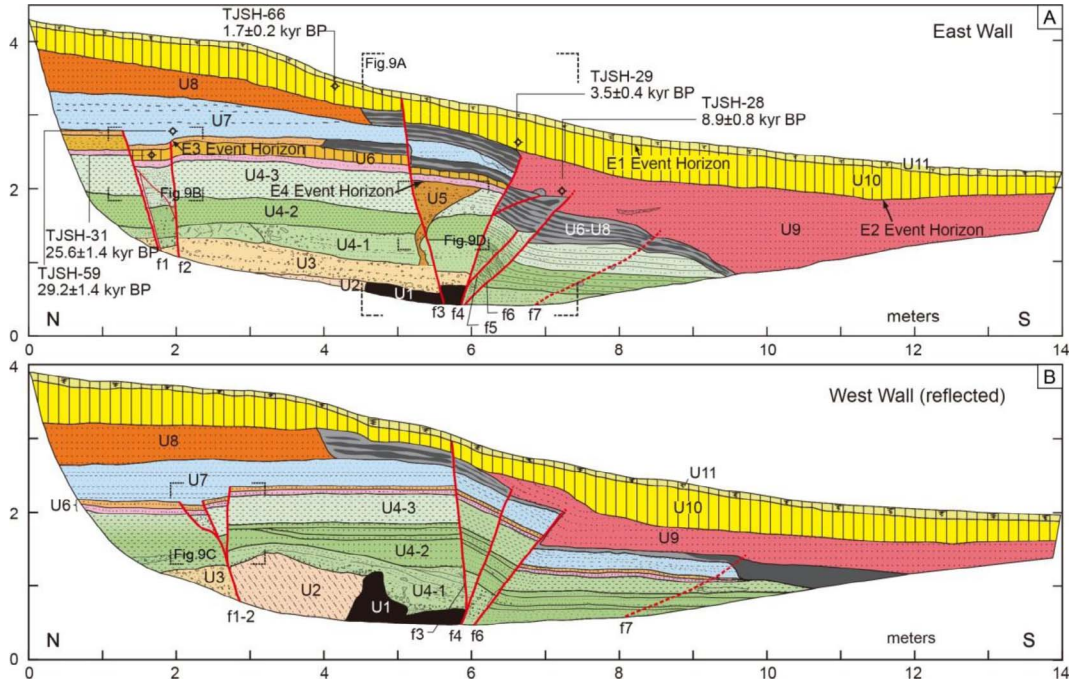

Fig. 8. Trench logs of the east (A) and west (B, reflected) walls of TC-5, depicting the stratigraphy and deformation associated with the interpreted earthquake events, E1 through E4. Faults are shown with thick red lines. Sedimentary units are indicated by different colors and are labeled numerically (see detail in Table S1). Stratigraphic positions of OSL samples are shown by black circles. Liquefaction is only observed on the east wall; note how U5 is deformed. Dashed corners correspond to the outlines of photographs in Fig. 9. See Section 3.2.2 for descriptions of the evidence for the individual earthquake events. (For interpretation of the references to colour in this figure legend, the reader is referred to the web version of this article.)

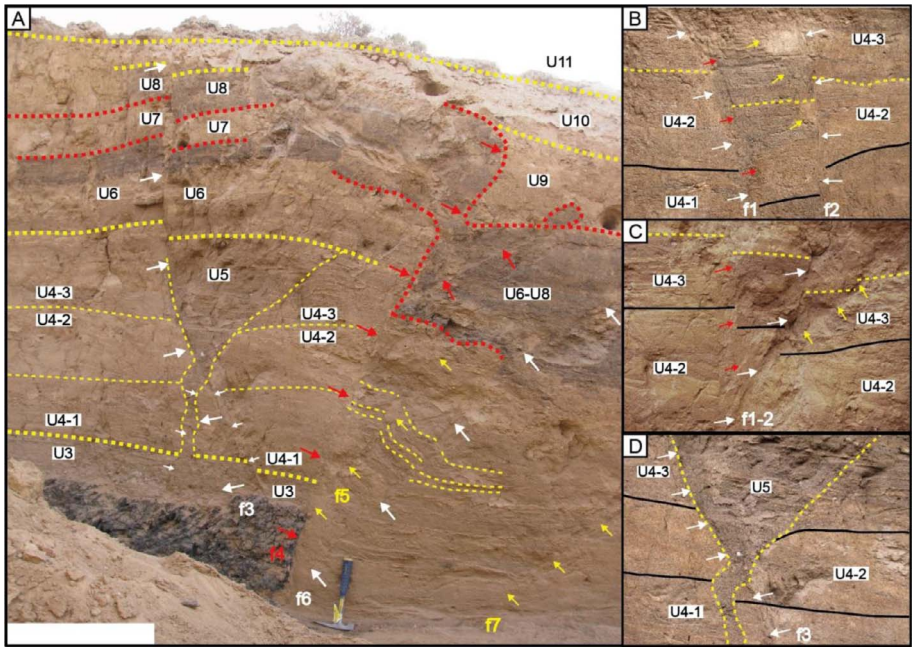

Fig. 9. Photographs of parts of the east and west walls of TC-5, showing evidence for the interpreted earthquake events, E1 through E4. (A) The fault f3 that offsets unit U7 (left side) provides the evidence for E1. E2 is characterized by several fault strands offsetting and folding the well-layered strata (right side). (B and C) Evidence for E3 is indicated by small grabens on both walls of the trench. (D) Liquefaction of unit U5 provides the evidence for E4, which is the oldest earthquake revealed in this trench.

displacement is not clear. Additionally, the age of OSL sample TJSH-59 (29.2 ± 1.4 kyr BP) is stratigraphically inverted with the younger age of OSL sample TJSH-31 (25.6 ± 1.4 kyr BP) in sediment clearly broken by faults f1 and f2. If sample TJSH-59 in unit U7 was deposited after displacement on faults f1 and f2, it may at best be interpreted that the antepenultimate displacement occurred somewhere around 25–29 kyr BP.

The oldest earthquake (E4) is indicated by a fault-controlled wedge, unit U5, filled with coarse sand and fine-grained pebbles within unit U4-3; the lower part of this wedge links to liquefied strata of unit U3 via a tube-like dike (Figs. 8 and 9D). The lower contact of the overlying unit, U6, is well-preserved and is expressed as a continuous, flat, silty layer, showing no noticeable liquefaction effect. In addition, stratigraphic thickness changes of units U1 and U3 across f3 indicate that an older strike-slip displacement may also have occurred on f3. Therefore, the oldest earthquake can reasonably be inferred to have occurred sometime between the deposition of unit U4-3 and unit U6.

The sequence of displacement and accompanying erosion in the trench is summarized in Fig. 10. The cumulative vertical displacement of all the earthquake horizons is ~0.85 m, consistent with the scarp height (0.77 ± 0.03 m) obtained from topographic survey profiles across the main fault zone. From this observation, it may be inferred that trench TC-5 preserves a complete record of paleoseismic events since E4.

3.2.3. TC-7

The TC-7 trench is located approximately 300 m south of the Dingwu Highway, which runs subparallel to the east–west trending fault trace (Figs. 1C and 11A). At the trench site, the surface trace of the Zhongwei subsegment (F4) follows the boundary between Neogene bedrock and late Quaternary sediments (Fig. 11A). The TC-7 trench is approximately 13 m long and was excavated across a discrete scarp that accommodated up to 3 m of south-side-up vertical slip (Fig. 11B–D). Exposed within the trench are four steeply dipping faults, designated as f1, f2, f3, and f4. The southernmost fault, f1, is confined within the Neogene bedrock. The remaining three fault strands break through and are associated with a sequence of late Pleistocene–Holocene colluvial and fill deposits, designated as units U2 through U7. Unit descriptions accompanying the trench log are shown in Supplementary Table 1. The structure and stratigraphy are interpreted to record six paleoearthquakes.

The most recent paleoearthquake (E1) is evident from the preservation of a wedge-shaped colluvial deposit (U7-1) bounded to the south by fault f2 (Fig. 12). This event occurred after deposition of units U6-2 and U5. OSL ages of samples TJSH-36, -37, and -38, taken from units U6-2 and U5, range from 8.2 ± 0.5 kyr BP to 11.0 ± 0.9 kyr BP and place a maximum bound on the age of E1. A penultimate event (E2) is recorded by another colluvial wedge unit U6-1, also bounded to the south by fault f2 (Fig. 12). Formation of the colluvial wedge unit, U6-1, occurred prior to deposition of the overlying unit, U6-2, and after deposition of the directly underlying unit, U5. The OSL age of sample TJSH-36, taken from overlying unit U6-2, is 11.0 ± 0.9 kyr BP. The OSL ages of samples TJSH-37 and TJSH-38, taken from underlying unit U5, are 9.9 ± 0.5 kyr BP and 8.2 ± 0.5 kyr BP, respectively. The ages of the underlying and overlying units are stratigraphically inverted. We assume that the older age of sample TJSH-36 is due to incomplete light exposure. Considering this assumption, the E1 and E2 paleoearthquake displacements postdate approximately 9.9 ± 0.5 kyr BP. An antepenultimate event (E3) is recorded by rupture of the base of unit U5 along fault strands f3 and f4. OSL samples TJSH-37 and TJSH-38 place the age of the lower portion of unit U4 somewhere around 9.9 ± 0.5 kyr BP and 8.2 ± 0.5 kyr BP, respectively; therefore, the antepenultimate event occurred after ~9.9 ± 0.5 kyr BP. In this regard, the trench exposure records three earthquake displacements since ~9.9 ± 0.5 kyr BP, but provides no unique information to place either upper or lower bounds on the timing of each displacement.

An older paleoearthquake (E4) is recorded by colluvial wedge unit U4. Formation of colluvial wedge U4 postdates deposition of unit U3-2, which is dated at 24.3 ± 2.1 kyr BP (OSL sample TJSH-61), and likely predates the depositional age of OSL sample TJSH-38 (8.2 ± 0.5 kyr BP) in unit U5. A small fissure-fill–colluvial deposit unit U3-1, which abuts fault strand f3, is interpreted to record an even older paleoearthquake (E5). The deposition of unit U3-1, and thus the age of E5, postdates deposition of unit U2-3, which has an age of approximately 32.5 ± 1.3 kyr BP to 28.1 ± 1.6 kyr BP (OSL ages of samples TJSH-49 and -39, respectively) and predates the depositional age of unit U3-2, dated at 24.3 ± 2.1 kyr (TJSH-61). The colluvial wedge deposit U2-1, abutting fault strand f2, records the oldest paleoearthquake (E6) interpreted in the trench exposure. We have no OSL ages to place a maximum bound on the timing of E6. The 32.5 ± 1.3 kyr BP age of OSL sample TJSH-49, taken from unit U2-3, places a minimum bound on the age of event E6.

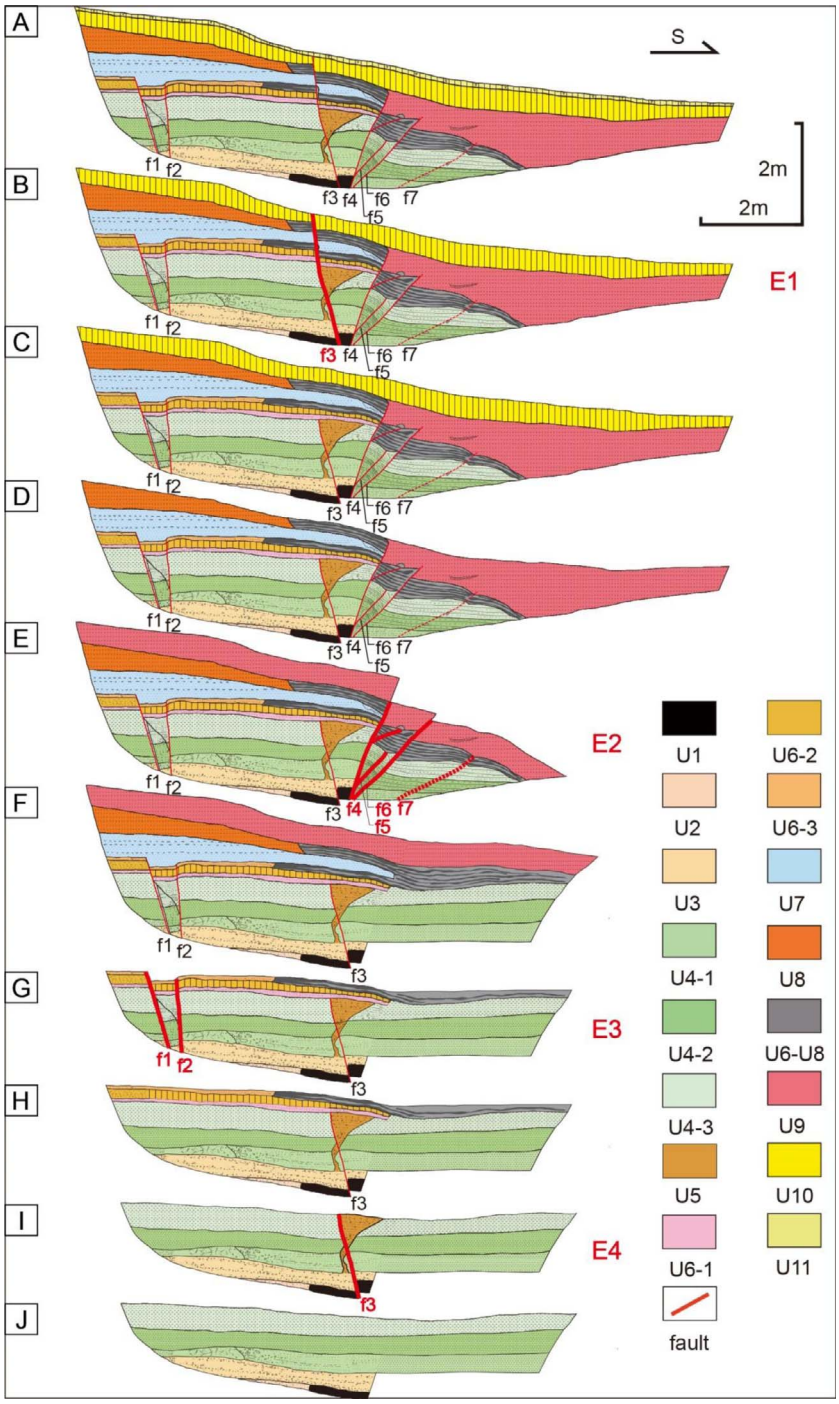

Fig. 10. Possible restoration of the stratigraphy on the east wall of trench TC-5, showing the deformation associated with events E1 to E4. (A) Present-day situation after the deposition of U11; (B) E1, rupturing of the most recent earthquake along f3 and fault scarp formation; (C) Deposition of U10; (D) Erosion of U9 on the upthrown wall and deposition of U9 on the downthrown wall; (E) E2, rupturing of the penultimate earthquake along f4–f7 simultaneously and geomorphic scarp formation; (F) Successive deposition of U7–U9; (G) E3, formation of small extensional graben between f1 and f2; (H) Deposition of U6; (I) E4, liquefaction and fault-controlled sand funneling and channeling; (J) Possible original situation and the successive deposition of U2–U4.

Six of the interpreted events, E1 through E6, appear to be large surface-rupturing earthquakes. The cumulative vertical displacement for these paleoearthquakes is approximately 3.2 m, determined through restoration of the strata deposited before and after each event (Fig. 13), which is consistent with the scarp height of 3.17 ± 0.3 m obtained from topographic survey profiles across the main fault zone. Therefore, trench TC-7 likely records a complete sequence of paleoseismic events since E6.

3.3. Slip rate estimation of the western Tianjingshan fault

A displaced stream channel near the TC-5 trench site (Fig. 7) affords an opportunity to establish the fault slip rate. There are two stream channels incised into the hanging wall at this site (Fig. 14). The eastern of the two hanging wall channels is only ~30 m long, narrow in width, and is not well developed, as evidenced by a knickpoint at its head where headward erosion is actively migrating up the faulted alluvial fan surface (Fig. 7D). The older stream channel within the alluvial fan at this site extends ~700 m upward into Pleistocene alluvial deposits and downstream to where it feeds into the Majiajing River (Fig. 7B). The two drainages join in the footwall. The smaller channel displays a 2.7 m left-lateral offset in the channel wall. The older channel in the hanging wall is offset by approximately 11.7 ± 0.5 m (Fig. 14B). Support for the correlation and offset is further found in the observation that the profiles of the older stream channel on both sides of the fault match very well. In addition to the horizontal offset, vertical offsets of 0.74 ± 0.12 m and 0.80 ± 0.12 m are obtained by measuring the offsets of two topographic profiles across the north-side-up fault scarp

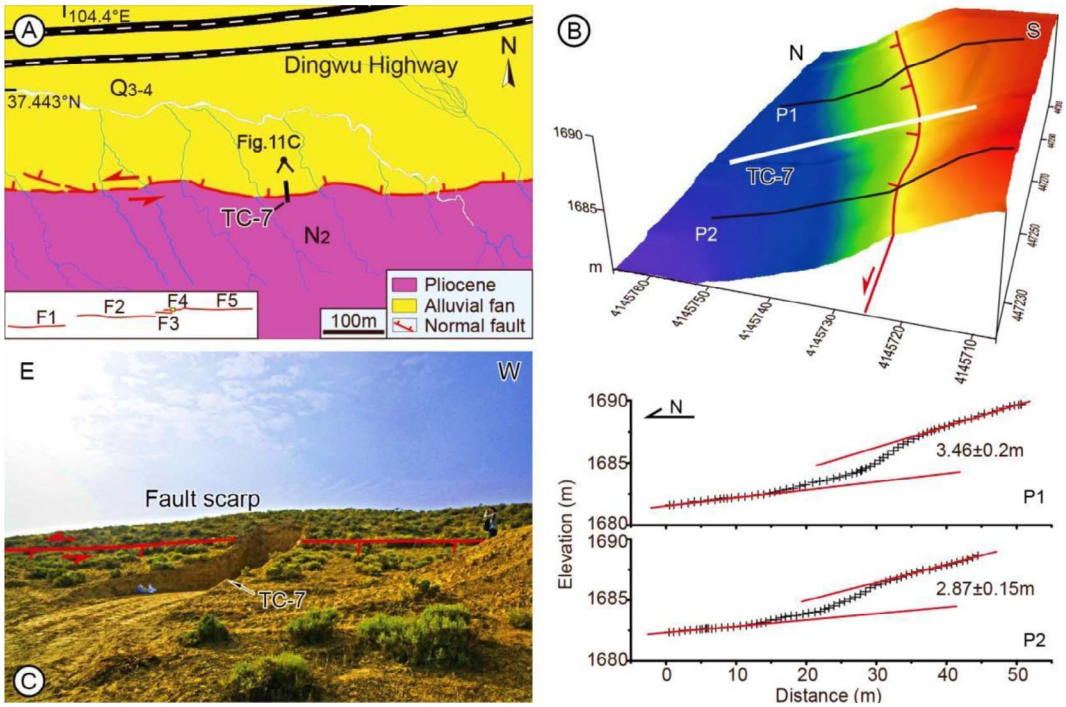

Fig. 11. Geomorphological mapping and features of the central portion of F4 (Zhongwei subsegment). (A) Morphotectonic map showing the fault trace, geomorphological units, and stream channels. Location is shown in the lower-left corner sketch map. Black bar shows the location of trench TC-7 (37.441709°N, 104.403813°E). (B) 3-D model showing the fault scarp and trench site, created using high-resolution differential GPS (DGPS) surveying. Profiles (P1 and P2) across the fault zone show scarp heights of ~3.46 m and ~2.87 m, respectively. (C) South-looking view of the fault scarp and TC-7 trench site. Location is shown in (A).

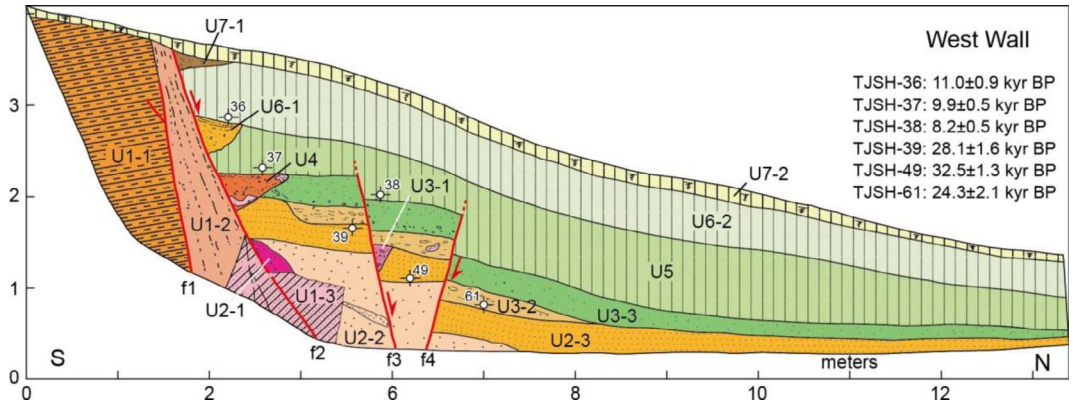

Fig. 12. Trench log of the west wall of TC-7, depicting the stratigraphy and deformation associated with the interpreted earthquake events, E1 through E6. Red lines indicate fault strands. Sedimentary units are indicated by different colors and are labeled numerically (see detail in Table S1). Stratigraphic positions of OSL samples are shown by black circles. See Section 3.2.3 for descriptions of the evidence for the individual earthquake events. (For interpretation of the references to colour in this figure legend, the reader is referred to the web version of this article.)

(Fig. 7C). The alluvial fan surface into which the 11.7-m-offset channel incises is capped by an ~0.5 m thick layer of loess. We interpret that the alluvial deposits at the base and below the loess layer represent the times of stream incision initiation and fan surface abandonment, respectively. An OSL sample (TJSH-65; Supplementary Table 2), collected in a ~0.8 m hand-excavated hole at the topmost section of the sand layer on the alluvial fan (Figs. 7D and 14A), places the age of abandonment at 10.7 ± 1.0 kyr BP. This age places a maximum bound on the time at which the larger stream was incised and began to record lateral offset. Dividing the observed 11.7 ± 0.5 m offset by the age of fan abandonment at 10.7 ± 1.0 kyr BP places a minimum value on the fault slip rate equal to 1.1 ± 0.1 mm/yr. Similarly, the vertical fault slip rate is estimated at 0.2 ± 0.1 mm/yr.

4. Discussion

The observations from our trenching studies are summarized in the form of a space–time diagram in Fig. 15. The relative location of each trench along the fault zone is marked along the horizontal axis and the boxes show the temporal constraints on the timing of earthquakes we obtained from our trenching studies. Other researchers have also conducted trenching studies along the fault (Chen et al., 2006; Du et al., 2007; Unpublished results, IGCEA et al., 2003; Min et al., 2001) and their results are included in the plot in Fig. 15. Within the limits of dating paleoearthquakes at each site, the data allow us to infer that the entirety of the fault zone ruptured during the most recent earthquake. The period 1.1–1.3 kyr BP, corresponding to the thickness of the red line in Fig. 15, is the single time period that satisfies the timing of the most recent paleoearthquake at the 10 trench sites. If this is true, the majority of data allow us to suggest that the most recent event occurred

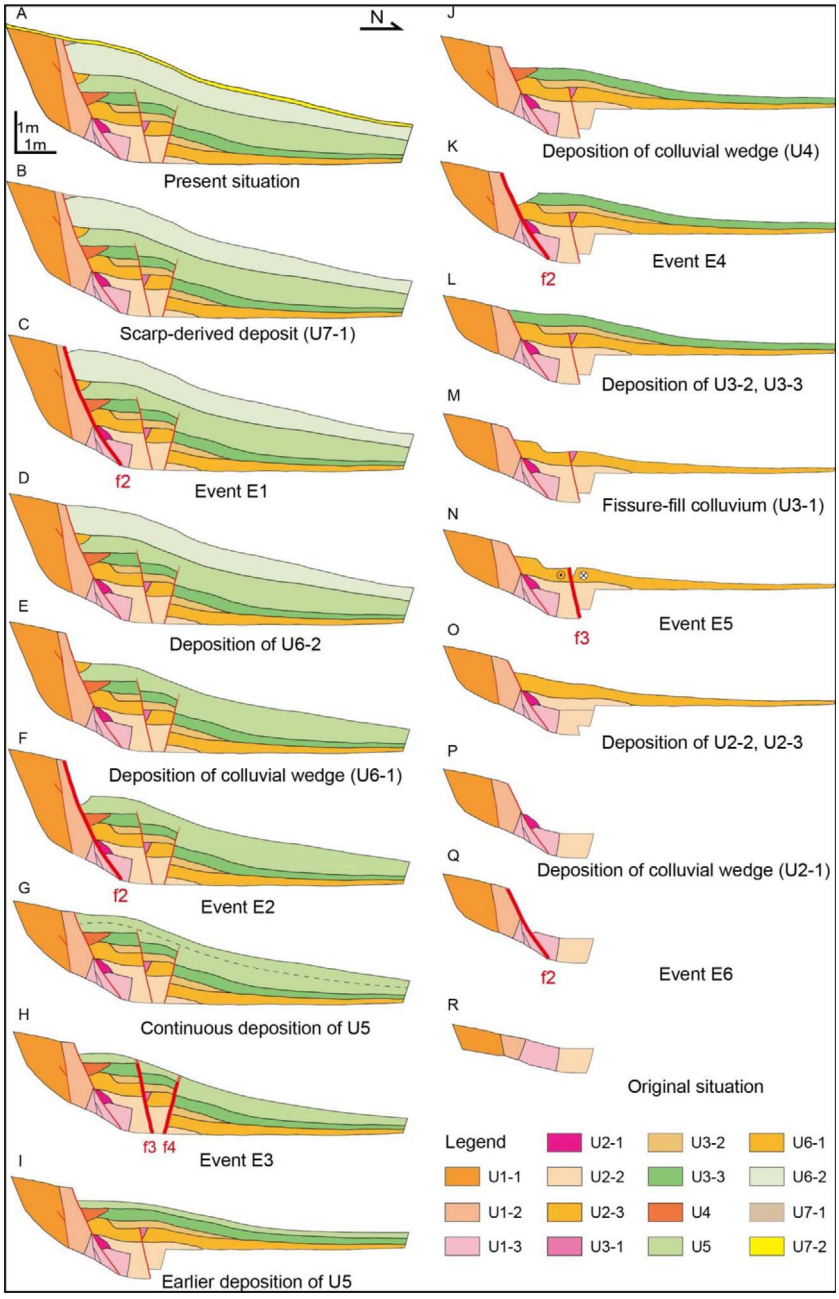

Fig. 13. Possible restoration of the stratigraphy on the west wall of trench TC-7, showing the deformation associated with events E1 to E6. (A) Present situation after the deposition of U7-2; (B) Post-faulting deposition of U7-1; (C) E1, rupturing of the most recent earthquake along f2; (D) Deposition of U6-2; (E) Post-faulting deposition of colluvial wedge unit U6-1; (F) E2, rupturing along f2 and scarp formation; (G) Continuous deposition of U5 after earthquake event E3; (H) E3, rupturing along f3 and f4; (I) Earlier deposition of U5; (J) Post-faulting deposition of colluvial wedge unit U4; (K) E4, rupturing along f2 and scarp formation; (L) Deposition of U3-2 and U3-3; (M) Post-faulting deposition of fissure-fill colluvium unit U3-1; (N) E5, rupturing along f3; (O) Deposition of U2-2 and U2-3; (P) Post-faulting deposition of colluvial wedge unit U2-1; (Q) E6, rupturing along f2 and scarp formation; (R) Possible original situation.

approximately between 1.1 and 1.3 kyr BP, and not at the same time as the historical 1709 earthquake that has been documented on the C-TJSF (Nie and Lin, 1993; W.Q. Zhang et al., 1988; Zhang et al., 2015; Fig. 1B). Though numerous trenches have now been excavated along the W-TJSF, constrains on the timing of the penultimate and older earthquakes remain limited. The largest number of paleoearthquakes is observed in trench TC-7, where six surface-rupturing earthquakes are recorded over the last ~35 kyr. If these values are representative of the entire W-TJSF, and the fault always breaks in its entirety, it appears that the average return time of surface-rupturing earthquakes is approximately 5000 yr. If the fault does not always break along its entire length, then the occurrence rate of surface-rupturing earthquakes will accordingly be more frequent, and their rupture lengths and magnitudes respectively smaller.

The length of the W-TJSF (e.g., Fig. 1C) provides a basis to place limits on the size of past earthquakes on the fault zone. The length of the W-TJSF is approximately 60 km. If it is assumed that the entire fault ruptures, one may use published scaling relationships between earthquake magnitude and rupture length. Using the regressions of Wells and Coppersmith (1994) and Wesnousky (2008), entire rupture of the W-TJSF will produce an earthquake of magnitude and moment equal to 7.15 and 6.3 × 10^{26} dyne·cm, respectively. The same approach can be used with the measures of repeated offset summarized in Fig. 3, which suggests that offsets average ~3 m when the W-TJSF ruptures. Using the regressions of Wells and Coppersmith (1994) and Wesnousky (2008), a rupture with average surface offset of ~3 m corresponds to an earthquake of magnitude and moment equal to 7.47 and 3 × 10^{27} dyne·cm, respectively. One may also compute the expected seismic moment of an earthquake rupturing the entire 60 km length of the W-TJSF. The formulation for seismic moment = uLWD, where μ is the crustal rigidity (3 × 10^{11} dyne/cm^2), L is the fault length, W is the fault width, and D is the average displacement. Assuming that the fault width is 15 km (Gao et al., 2013), which is the approximate depth of the seismogenic layer for continental earthquakes, the length is 60 km, and the average displacement is 3 m, the expected seismic moment is 8.1 × 10^{26} dyne·cm, or Mw = ~7.2.

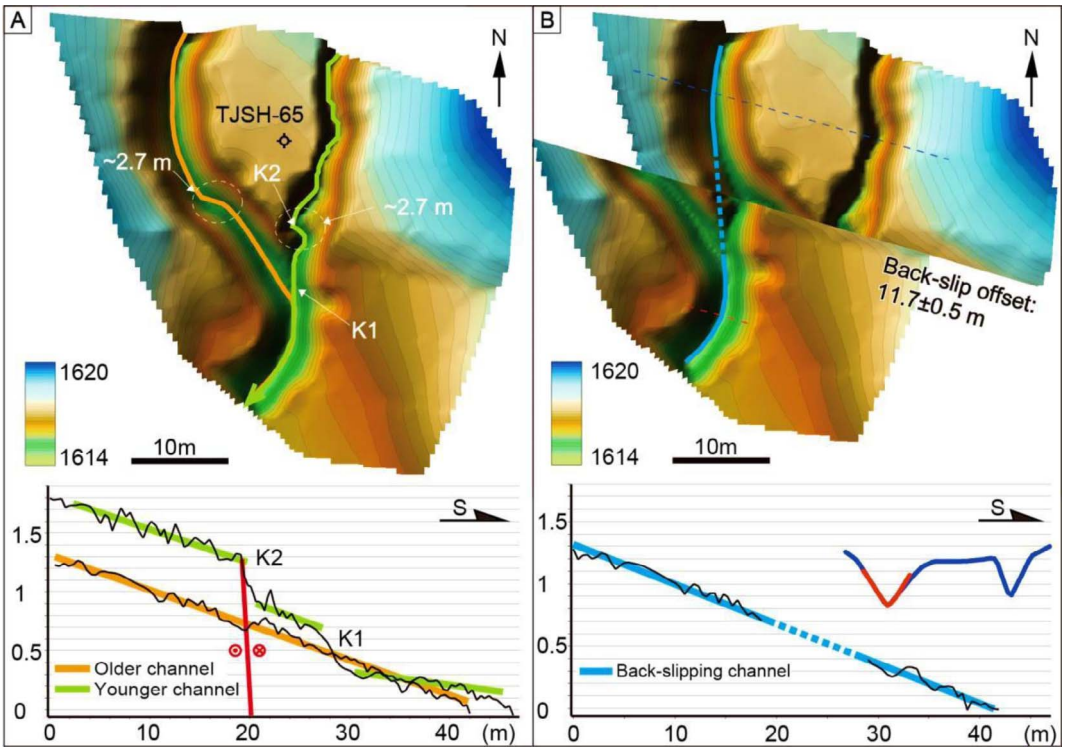

Fig. 14. Stream offset reconstruction at the Majiajing site. (A) Topographic map of displaced stream channels and longitudinal profiles showing the possible fault geometry and vertical displacement of ~0.3 m. Knickpoints are labeled as K1 and K2. (B) Retro-deforming the image by ~11.7 ± 0.5 m along the fault trace realigns the older stream channel and west edge of the fan. The cross-sections along the dashed red and blue lines projected onto the fault plane show the well-matched upstream and downstream channels. (For interpretation of the references to colour in this figure legend, the reader is referred to the web version of this article.)

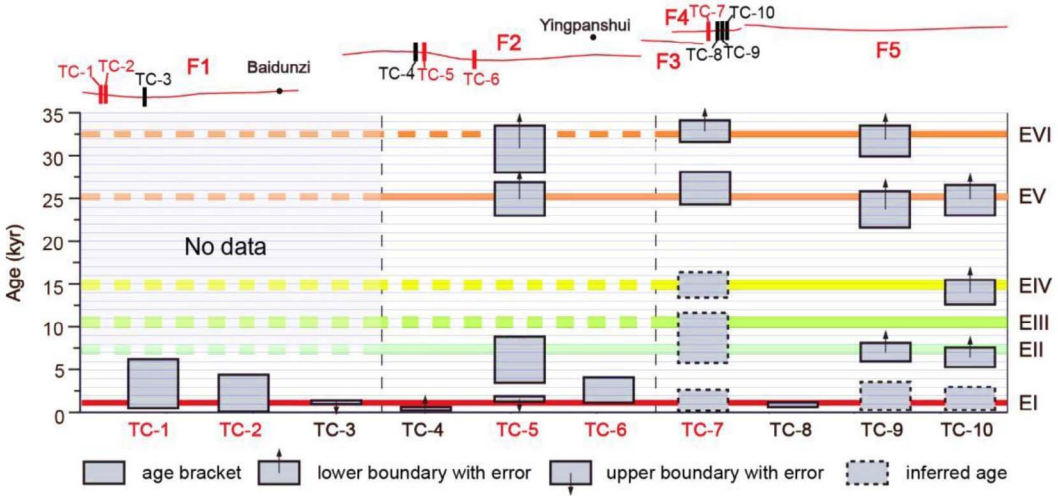

Fig. 15. Paleoearthquake sequence constrained by trenching investigations (Chen et al., 2006; Du et al., 2007; Unpublished results, IGCEA et al., 2003; Min et al., 2001; this study) along the W-TJSF. Red lines indicate the fault strands. (Upper) Map showing the geometric pattern of the five fault segments and trench locations along the W-TJSF. Red bars are trenches excavated in this study. Black bars are trenches excavated in previous studies. (Lower) Temporal and spatial patterns of paleoearthquakes that occurred along the W-TJSF. From youngest to oldest, the events on the western segment are named EI, EII, EIII, EIV, EV, and EVI. Note that EI corresponds to the most recent earthquake at ~1.2 kyr BP, which completely ruptured the W-TJSF. (For interpretation of the references to colour in this figure legend, the reader is referred to the web version of this article.)

The slip rate of > 1.1 mm/yr we calculate for the segment of the western Tianjingshan fault is comparable to fault slip rates of ~2.5 mm/yr and 0.7–1.6 mm/yr proposed by previous studies on the central and eastern segments of the Tianjingshan fault, respectively (Chai et al., 1997; Li, 2005). These values are also in agreement with the present-day GPS velocity of ~1–1.3 mm/yr along the Tianjingshan fault (Gan et al., 2007; Li et al., 2009; Zheng et al., 2013). Results from deep seismic reflection profiles suggest that the Tianjingshan fault developed as a result of northeastward migration of a large thrust ramp, and that it merges with, and initiated subsequent to the Haiyuan fault, dipping SW at shallow angle in the middle–lower crust (Gao et al., 2013). Thus, the Tianjingshan fault and the Haiyuan fault together accommodate left-lateral slip and crustal shortening along the northeasternmost margin of the Tibetan Plateau deriving from the collision and subsequent indentation of India into Eurasia. The left-lateral Haiyuan and Altyn Tagh faults are inferred to be major intracontinental boundary faults that control the eastward extrusion of rigid blocks, with poorly constrained geologic slip rates of ~12–20 mm/yr and ~20–30 mm/yr, respectively (Gaudemer et al., 1995; Lasserre et al., 1999, 2002; Meyer et al., 1998; Mériaux et al., 2004, 2005; Peltzer

et al., 1989). However, numerous geologic (e.g., Cowgill, 2007; Cowgill et al., 2009; Li et al., 2009; Yuan et al., 1998; P.Z. Zhang et al., 1988; Zhang et al., 2007), GPS (e.g., Bendick et al., 2000; Li et al., 2009; Loveless and Meade, 2011; Shen et al., 2001; Thatcher, 2007; Wallace et al., 2004; Zhang et al., 2004; Zheng et al., 2013), and InSAR (e.g., Cavalié et al., 2008; Elliott et al., 2008) studies suggest that the slip rates of the Haiyuan and Altyn Tagh faults are ~4–6 mm/yr and ~10 mm/yr, respectively. It is important to note that the sum of the slip rates of the Tianjingshan fault and the Haiyuan fault (5–7 mm/yr) is only ~30–50% of that assumed in the eastward extrusion model, and the same is true along the Altyn Tagh fault. Therefore, our observations are more likely to favor a lower slip-rate model, whereby crustal deformation in NE Tibet not only partitions along major strike-slip faults, but may also be accommodated by internal ductile deformation.

5. Conclusions

Our offset measurements record up to six surface-rupturing events on the W-TJSF, with a similar coseismic slip of 3–4 m for successive earthquakes. Trenching investigations along the W-TJSF further suggest that approximately six paleoearthquakes may have occurred during the last 35 kyr, with an average Holocene earthquake recurrence interval of ~5000 yr. The most recent earthquake on the W-TJSF occurred ~1.2 ± 0.1 kyr BP, indicating that the W-TJSF did not experience surface rupture during the 1709 earthquake that is known to have ruptured the C-TJSF. Here, we provide the first quantitative slip-rate estimate (1.1–1.2 mm/yr) for the W-TJSF. The relatively high slip rate of the Tianjingshan fault shows that it is important in accommodating the sinistral displacement and crustal shortening deformation in NE Tibet.

Acknowledgments

This work was jointly supported by the National Science Foundation of China (41590861, 41661134011, 41372220, and 41472200), the Public Service Funds for Earthquake Studies (201408023) and the Fundamental Research Funds of the Institute of Geology, China Earthquake Administration (IGCEA1220). We thank Olaf Zielke and Zhikun Ren for comments that improved a previous version of the manuscript, and Stephen J. Angster for his help with the language of the manuscript. We thank Longsheng Zhang and Hongdong Wang for their help during field work, and Changsheng Wang for his help in processing the OSL dating samples. We would also like to express our sincere appreciation to Prof. Daoyang Yuan, an anonymous reviewer, and the editor Dr. Michel Faure, whose insightful and constructive comments improved this manuscript.

Appendix A. Supplementary material

Supplementary data associated with this article can be found, in the online version, at http://dx.doi.org/10.1016/j.jseaes.2017.04.031.

References

Bendick, R., Bilham, R., Freymueller, J., Larson, K., Yin, G., 2000. Geodetic evidence for a low slip rate in the Altyn Tagh fault system. Nature 404 (6773), 69–72. http://dx.doi.org/10.1038/35003555.

Cavalié, O., Lasserre, C., Doin, M.P., Peltzer, G., Sun, J., Xu, X., Shen, Z.K., 2008. Measurement of interseismic strain across the Haiyuan fault (Gansu, China), by InSAR. Earth Planet. Sci. Lett. 275 (3), 246–257. http://dx.doi.org/10.1016/j.epsl.2008.07.057.

Chai, C.Z., Zhang, W.Q., Jiao, D.C., 1997. Discussion of the level active severity in different time intervals and segments on late Quaternary along Tianjingshan fault zone. Earthquake Res. China 13 (1), 35–42.

Chai, C.Z., Jiao, D.C., Liao, Y.H., Zhang, S.Y., Du, P., Shen, W.H., 2003. Discovery of surface rupture zone produced by Guanguanling earthquake at the juncture of Ningxia, Inner Mongolia and Gansu Province. Seismol. Geol. 25 (1), 167–171.

Chen, G.X., Tian, Q.J., Zhou, B.G., Min, W., Liu, B.J., Gao, Z.W., 2006. Some seismogeological questions regarding to Daliushu Dam Site in Heishanxia Valley of Yellow River. Technol. Earthquake Disaster Prevent. 1 (3), 186–198.

Cowgill, E., 2007. Impact of riser reconstructions on estimation of secular variation in rates of strike-slip faulting: revisiting the Cherchen River site along the Altyn Tagh Fault, NW China. Earth Planet. Sci. Lett. 254, 239–255. http://dx.doi.org/10.1016/j.epsl.2006.09.015.

Cowgill, E., Gold, R.D., Xuanhua, C., Xiao-Feng, W., Arrowsmith, J.R., Southon, J., 2009. Low Quaternary slip rate reconciles geodetic and geologic rates along the Altyn Tagh fault, northwestern Tibet. Geology 37 (7), 647–650. http://dx.doi.org/10.1130/G25623A.1.

Du, P., Chai, C.Z., Shen, W.H., Min, W., Tian, Q.J., 2007. Characteristics of the Holocene activity of the Guanguanling fault zone. Seismol. Geol. 29 (3), 597–606.

Elliott, J.R., Biggs, J., Parsons, B., Wright, T.J., 2008. InSAR slip rate determination on the Altyn Tagh Fault, northern Tibet, in the presence of topographically correlated atmospheric delays. Geophys. Res. Lett. 35, L12309. http://dx.doi.org/10.1029/2008GL033659.

Gan, W.J., Zhang, P.Z., Shen, Z.K., Niu, Z.J., Wang, M., Wan, M.G., Zhou, D.M., Cheng, J., 2007. Present-day crustal motion within the Tibetan Plateau inferred from GPS measurements. J. Geophys. Res. 112 (B8). http://dx.doi.org/10.1029/2005JB004120.

Gao, R., Wang, H.Y., Yin, A., Dong, S.W., Kuang, Z.Y., Zuza, A.V., Li, W.H., Xiong, X.S., 2013. Tectonic development of the northeastern Tibetan Plateau as constrained by high-resolution deep seismic-reflection data. Lithosphere 5 (6), 555–574. http://dx.doi.org/10.1130/L293.1.

Gaudemer, Y., Tapponnier, P., Meyer, B., Peltzer, G., Guo, S., Chen, Z., Dai, H., Cifuentes, I., 1995. Partitioning of crustal slip between linked, active faults in the eastern Qilian Shan, and evidence for a major seismic gap, the 'Tianzhu gap', on the western Haiyuan Fault, Gansu (China). Geophys. J. Int. 120 (3), 599–645.

Gu, G.X., Lin, T.H., Shi, Z.L., 1983. Catalogue of Chinese Earthquakes (1831 BC–1969 AD). Science Publishing House, Beijing.

Unpublished results, Institute of Geophysics, CEA., Center for Analysis and Prediction, SSB., Institute of Geology, CEA., Institute of Crustal Dynamics, CEA., Center for Geophysical Exploration, CEA., 2003. Seismogeological supplementary work report at Heishanxia section of the Yellow River.

Klinger, Y., Etchebes, M., Tapponnier, P., Narteau, C., 2011. Characteristic slip for five great earthquakes along the Fuyun fault in China. Nat. Geosci. 4 (6), 389–392. http://dx.doi.org/10.1038/ngeo1158.

Lasserre, C., Morel, P.H., Gauudemer, Y., Tapponnier, P., Ryerson, F.J., King, G.C.P., Métivier, F., Kasser, M., Kashgarian, M., Liu, B., Lu, T., Yuan, D., 1999. Postglacial left slip rate and past occurrence of M≥8 earthquakes on the western Haiyuan fault, Gansu, China. J. Geophys. Res. 104, 17633–17651. http://dx.doi.org/10.1029/1998JB900082.

Lasserre, C., Gaudemer, Y., Tapponnier, P., Mériaux, A.S., Van der Woerd, J., Daoyang, Y., Ryerson, F.J., Finkel, R.C., Caffee, M.W., 2002. Fast late Pleistocene slip rate on the Leng Long Ling segment of the Haiyuan fault, Qinghai, China. J. Geophys. Res. 107 (B11), 2276. http://dx.doi.org/10.1029/2000JB000060.

Li, C.Y., 2005. Quantitative Studies on Major Active Fault Zones in Northeastern Qinghai-Tibet Plateau. Institute of Geology, CEA, Beijing (PhD thesis).

Li, C.Y., Zhang, P.Z., Yin, J.H., Min, W., 2009. Late Quaternary left-lateral slip rate of the Haiyuan fault, northeastern margin of the Tibetan Plateau. Tectonics 28 (TC5010). http://dx.doi.org/10.1029/2008TC002302.

Li, X.N., Li, C.Y., 2015. Characteristic slip behavior analysis of the western segment of the Xiangshan-Tianjingshan fault zone since late Quaternary. Seismol. Geol. 37 (2), 482–495. http://dx.doi.org/10.3969/j.issn.0253-4967.2015.02.011.

Loveless, J.P., Meade, B.J., 2011. Partitioning of localized and diffuse deformation in the Tibetan Plateau from joint inversions of geologic and geodetic observations. Earth Planet. Sci. Lett. 303 (1), 11–24. http://dx.doi.org/10.1016/j.epsl.2010.12.014.

Lu, Y.C., Wang, X.L., Wintle, A.G., 2007. A new OSL chronology for dust accumulation in the last 130,000 yr for the Chinese Loess Plateau. Quatern. Res. 67 (1), 152–160. http://dx.doi.org/10.1016/j.yqres.2006.08.003.

Mériaux, A.S., Ryerson, F.J., Tapponnier, P., Van der Woerd, J., Finkel, R.C., Xu, X., Xu, Z., Caffee, M.W., 2004. Rapid slip along the central Altyn Tagh Fault: morphochronologic evidence from Cherchen He and Sulamu Tagh. J. Geophys. Res. 109, B06401. http://dx.doi.org/10.1029/2003JB002558.

Mériaux, A.S., Tapponnier, P., Ryerson, F.J., Xiwei, X., King, G., Van der Woerd, J., Finkel, R.C., Haibing, L., Caffee, M.W., Zhiqin, X., Wenbin, C., 2005. The Aksay segment of the northern Altyn Tagh fault: tectonic geomorphology, landscape evolution, and Holocene slip rate. J. Geophys. Res. 110, B04404. http://dx.doi.org/10.1029/2004JB003210.

Meyer, B., Tapponnier, P., Bourjot, L., Métivier, F., Gaudemer, Y., Peltzer, G., Shunmin, G., Chen, Z., 1998. Crustal thickening in Gansu-Qinghai, lithospheric mantle subduction, and oblique, strike-slip controlled growth of the Tibet Plateau. Geophys. J. Int. 135, 1–47. http://dx.doi.org/10.1046/j.1365-246X.1998.00567.x.

Min, W., Zhang, P.Z., Deng, Q.D., 2001. The study of Holocene paleoearthquakes on Zhongwei-Tongxin fault zone. Seismol. Geol. 23 (3), 357–366.

Nie, Z., Lin, W.F., 1993. Middle segment of the Zhongwei-Tongxin fault zone: seismic deformation band of 1709 earthquake with M=7 1/2 along Xiangshan-Tianjingshan fault zone. Earthquake 13 (1), 41–44.

Peltzer, G., Tapponnier, P., Armijo, R., 1989. Magnitude of late Quaternary left-lateral displacements along the north edge of Tibet. Science 246 (4935), 1285–1289. http://dx.doi.org/10.1126/science.246.4935.1285.

Shen, Z.-K., Wang, M., Li, Y., Jackson, D.D., Yin, A., Dong, D., Fang, P., 2001. Crustal deformation along the Altyn Tagh fault system, western China, from GPS. J. Geophys. Res. 106 (B12), 30607–30621. http://dx.doi.org/10.1029/2001JB000349.

Thatcher, W., 2007. Microplate model for the present-day deformation of Tibet. J. Geophys. Res. 112 (B1). http://dx.doi.org/10.1029/2005JB004244.

Wallace, K., Yin, G., Bilham, R., 2004. Inescapable slow slip on the Altyn Tagh fault.

Geophys. Res. Lett. 31, L09613. http://dx.doi.org/10.1029/2004GL019724.
Wang, Y.P., Song, F.M., Li, Z.Y., You, H.C., An, P., 1990. Study on recurrence intervals of great earthquakes in the Late Quaternary of Xiangshan-Tianjingshan fault zone in Ningxia. Earthquake Res. China 6 (2), 15–24.
Wells, D.L., Coppersmith, K.J., 1994. New empirical relationships among magnitude, rupture length, rupture width, rupture area, and surface displacement. Bull. Seismol. Soc. Am. 84 (4), 974–1002.
Wesnousky, S.G., 2006. Predicting the endpoints of earthquake ruptures. Nature 444 (7117), 358–360. http://dx.doi.org/10.1038/nature05275.
Wesnousky, S.G., 2008. Displacement and geometrical characteristics of earthquake surface ruptures: issues and implications for seismic-hazard analysis and the process of earthquake rupture. Bull. Seismol. Soc. Am. 98 (4), 1609–1632. http://dx.doi.org/10.1785/0120070111.
Yang, H.L., Chen, J., Thompson, J.A., Liu, J.F., 2012. Optical dating of the 12 May 2008, Ms 8.0 Wenchuan earthquake-related sediments: Tests of zeroing assumptions. Quat. Geochronol. 10, 273–279. http://dx.doi.org/10.1016/j.quageo.2012.02.022.
Yuan, D.Y., Liu, B.C., Lu, T.Y., He, W.G., Liu, X.F., Gan, W.J., 1998. Study on the segmentation in east segment of the northern Qilianshan fault zone. Northwestern Seismol. J. 20, 27–34.
Zhang, P.Z., Molnar, P., Burchfiel, B.C., Royden, L., Wang, Y.P., Deng, Q.D., Song, F.M., Zhang, W.Q., Jiao, D.C., 1988a. Bounds on the Holocene slip rate of the Haiyuan fault, North Central China. Quatern. Res. 30 (2), 151–164. http://dx.doi.org/10.1016/0033-5894(88)90020-8.
Zhang, P.-Z., Shen, Z., Wang, M., Gan, W., Bürgmann, R., Molnar, P., Wang, Q., Niu, Z., Sun, J., Wu, J., Sun, H., You, X., 2004. Continuous deformation of the Tibetan Plateau from global positioning system data. Geology 32, 809–812. http://dx.doi.org/10.1130/G20554.1.
Zhang, P.Z., Molnar, P., Xu, X., 2007. Late Quaternary and present-day rates of slip along the Altyn Tagh Fault, northern margin of the Tibetan Plateau. Tectonics 26, TC5010. http://dx.doi.org/10.1029/2006TC002014.
Zhang, W.Q., Jiao, D.C., Chai, C.Z., Song, F.M., Wang, Y.P., 1988b. Neotectonic features of the Xiangshan-Tianjingshan arc fracture zone and the seismic deformation zone of 1709 south of Zhongwei M = 7½ earthquake. Seismol. Geol. 10 (3), 12–20.
Zhang, W.Q., Jiao, D.C., Chai, C.Z., 2015. The Tianjingshan Active Fault Zone. Seismological Press, Beijing.
Zheng, W.J., Zhang, P.Z., He, W.G., Yuan, D.Y., Shao, Y.X., Zheng, D.W., Ge, W.P., Min, W., 2013. Transformation of displacement between strike-slip and crustal shortening in the northern margin of the Tibetan Plateau: Evidence from decadal GPS measurements and late Quaternary slip rates on faults. Tectonophysics 584, 267–280. http://dx.doi.org/10.1016/j.tecto.2012.01.006.
Zhou, J.X., Liu, B.C., 1987. The research of active Zhongwei-Tongxin fault. Northwestern Seismol. J. 9 (3), 71–77.
Zielke, O., Arrowsmith, J.R., Ludwig, L.G., Akçiz, S.O., 2010. Slip in the 1857 and earlier large earthquakes along the Carrizo Plain, San Andreas fault. Science 327 (5969), 1119–1122. http://dx.doi.org/10.1126/science.1182781.
Zielke, O., Klinger, Y., Arrowsmith, J.R., 2015. Fault slip and earthquake recurrence along strike-slip faults—contributions of high-resolution geomorphic data. Tectonophysics 638, 43–62. http://dx.doi.org/10.1016/j.tecto.2014.11.004.